Numerical modelling of the Storfjorden (Svalbard) polynya development due to wind stress: role of the sea ice rheology and damping forces

Denis Zyryanov, Jörg Haarpaintner & Reinert Korsnes

Remote sensing of the ice cover in Storfjorden (Svalbard) revealed the persistence and evolution of latent heat polynyas during the winter of 1997/98. Latent heat polynyas open mechanically under wind stress or ocean currents that transport the ice cover away. In the present work we used mathematical modelling to simulate the Storfjorden polynya size and geometry caused by wind stress, measured at the meteorological station on the island of Hopen in winter 1997/98. The dependence of the polynya outlines on the wind velocity is presented. Two approaches were used: quasi-static and dynamic. Quasi-static simulations are based on a time-independent, linear ice stress–strain relationship valid for the low strain rates only. Time dependence of the ice cover fracture is joined with stress–strain nonlinearity caused by ice delayed-elastic recovery and viscosity. Results are compared to satellite observations from the synthetic aperture radar (SAR) of ERS-2. The simulation results show that a northern wind opens a larger polynya (ca. 30 %) than does a north-eastern wind with the same speed. The results also indicate that the bathymetry and geometry of the fjord might have a stronger influence on the polynya opening and development than the location of individual islands and reefs.

D. Zyryanov, Institute of Water Problems, Russian Academy of Sciences, Gubkina st. 3, GSP-1 119991, Moscow, Russia, Denis.Zyryanov@aqua.laser.ru; J. Haarpaintner, Norwegian Meteorological Institute, Kirkegårdsveien 60, NO-9009 Tromsø, Norway; R. Korsnes, Norwegian Defence Research Establishment, Division of electronics, Box 25, NO-2027 Kjeller, Norway.

In the last ten years, sea ice dynamics challenges have been considered by means of discrete element models (DEM) (Hopkins 1993; Løset 1994; Hansen & Løset 1999a, 1999b) on different scales. The newly created DEM algorithms simulate sea ice ridging, ice destruction and ice drift in a dynamic approach based on complex underlying physics. Significantly increased computer performance makes the calculations easier and faster to execute. This paper continues the discrete element approach and demonstrates the simulation of the mesoscale sea ice cover destruction process.

The area of investigation was Storfjorden, a large fjord situated in the south-east of the Svalbard Archipelago between the islands of of Spitsbergen, Barentsøya and Edgeøya (Fig. 1). Synthetic aperture radar (SAR) from the European earth remote sensing satellite ERS-2 demonstrated the persistence of latent heat polynyas in this region. Haarpaintner (1999) described the evolution of a flaw polynya (between fast and pack ice) during the winter 1997/98 in Storfjorden and segmented the observed ice cover in the satellite images into fast ice, pack ice and polynyas. North-easterly winds were stated as the main

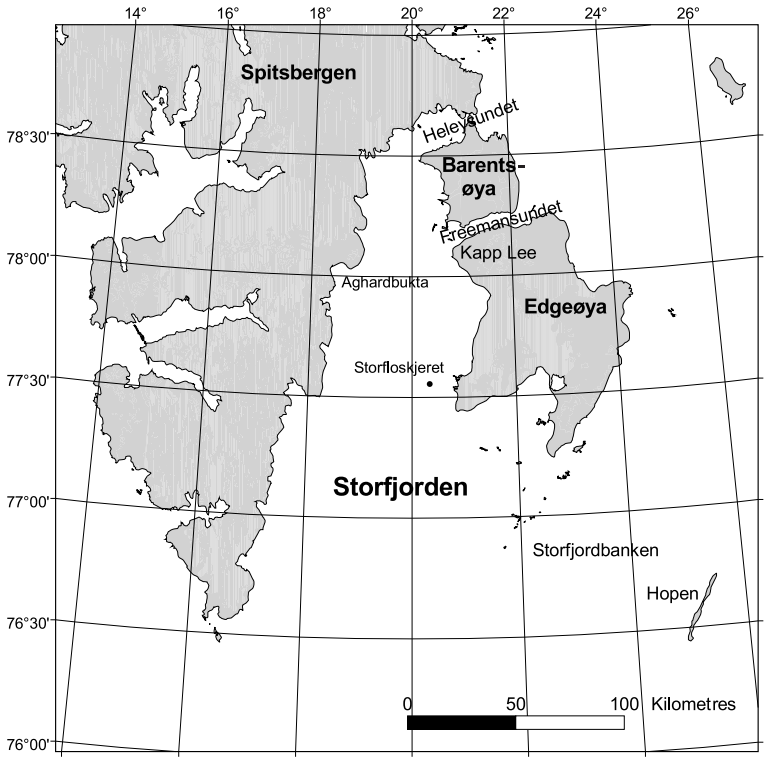

Fig. 1. Storfjorden is located in south-east Svalbard, between Spitsbergen, Barentsøya and Edgeøya.

reason for the existence of the latent heat polynya, but water currents and especially strong tidal currents through the two narrow sounds, Heleysundet and Freemansundet, in the north-east part of the fjord, may also play an important role in defining the polynya geometry. At its largest extent, the Storfjorden polynya reached an area of up to 6000 km^2. Covering on average only one sixth of Storfjorden, the polynyas were responsible for approximately two-thirds of the total 40 km^3 annual ice production in Storfjorden (Haarpaintner et al. 2001).

Since larger heat fluxes take place in polynyas and leads (Smith et al. 1990) than in Arctic pack ice, it is important to understand under which circumstances they develop. Latent heat polynyas open mechanically under wind stress or ocean currents that transport the ice cover away and when the advection of ice is blocked by land, reefs, fast ice or grounded ice on shallow shelves (Willmot et al. 1997). Important ice production takes place and under constant atmospheric conditions the polynya will reach an equilibrium size when ice export is balanced by ice production (Pease 1987).

In the following section we analyse the meteorological observations during the winter 1997/98 to determine the dominant wind direction and speed. The numerical modelling is outlined in subsequent sections. We consider two approaches: the quasi-static simulation, characterized by time independence, and the dynamic approach based on complex nonlinear sea ice rheology. The last section presents the simulation results and gives the quantitative assessments of the polynya size and geometry depending on wind stress, which are briefly compared to a manual segmentation of the ice cover in satellite observations. The sensitivity to possible wind force variations and different model parameters is discussed in Appendix 1.

Meteorological observations

As input wind stress data we use the averaged data from a station of the Norwegian Meteorological Institute on the island of Hopen (Fig. 1), since no in situ wind measurements were available from Storfjorden itself. The measurements were taken four times per day during the winter 1997/98. Figure 2 shows the daily averaged wind

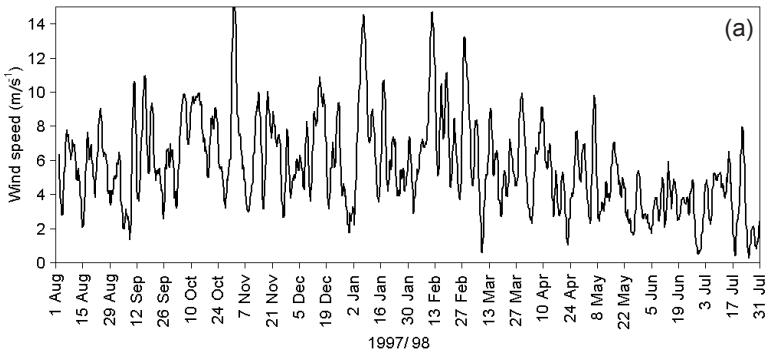

Fig. 2. (a) Daily averaged wind speed profile for the winter 1997/98. (b) Wind rose for the winter 1997/98. the dominant wind direction is from the north-east.

speed fluctuations and a wind rose for this time period. Although the wind conditions in Storfjorden might be locally influenced by the surrounding topography, simple ice drift modelling compared to ERS-2 SAR imagery showed that there is a strong correlation between the wind data measured on Hopen and the sea ice drift inside the fjord (Haarpaintner 1999). Observations showed that a first opening of the ice cover of ca. 2000 km^2 occurred at the end of January 1998 after three weeks of northerly winds of about 4 - 6 m/s. It closed again under the influence of southerly winds in the middle of February. We therefore assume that the overall wind conditions in this area are similar to the ones measured on Hopen. The maximum gusts measured during the winter 1997/98 were ca. 20.6 m/s. The average wind speed during winter was 6.1 m/s, whereas the dominant wind directions lie in the sector 0° N - 90° E (Fig. 2b).

The wind stress acting on the sea ice cover is calculated by:

$$\tau = C_D \cdot \rho_x \cdot u^2, \qquad (1)$$

where C_D is the surface drag coefficient, ρ_x is the air density and u represents the wind velocity. The air drag coefficient measured in the Arctic basin ranges from 1×10^{-3} to 3×10^{-3} (Banke & Smith 1973; Overland 1985, 1994). Omstedt et al. (1996) derived a drag coefficient of ca. 2.5×10^{-3} from theoretical explorations of wind force influencing the drifting ice. Thus, the wind speed of 4 - 6 m/s produces wind stress acting on the ice sheet in the range $(2 - 14) \times 10^4$ Nkm^{-2}. These estimates are used to calibrate the following numerical simulation. We will assume that the beginning of the sea ice cover destruction is directly correlated with the estimated wind stress magnitude. As we do not have any reliable information about the water currents inside Storfjorden, we neglect their possible influence on the polynya opening and limit our study on the wind drag.

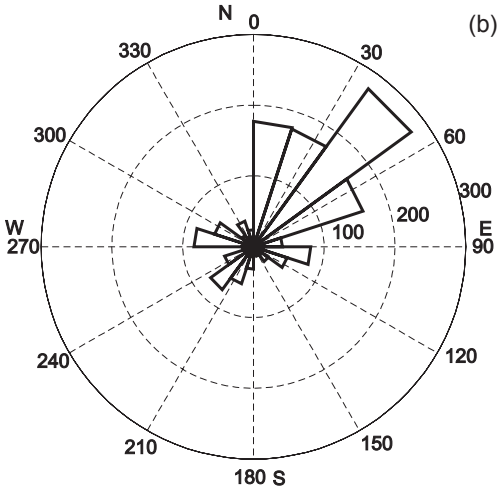

Disk-shaped rubble simulation

Our geomechanical model is based on the Particle Flow Code developed and supported by ITASCA Co. that is widely used in mining, environmental studies, the petroleum industry, the study of contaminants, waste elimination processes etc. The code deals with disk-shaped rubble particles, which can be bonded together to simulate solids and continuum media. This approach continues the DEM applied by several authors to the modelling of round ice floe movements and their interaction (Hopkins & Hibler 1991; Savage 1992; Løset 1994; Sayed et al. 1995; Hansen & Løset 1999a, 1999b), whereas Hopkins (Hopkins et al. 1991; Hopkins 1996) used irregularly shaped ice floes. The background theory for the DEM is

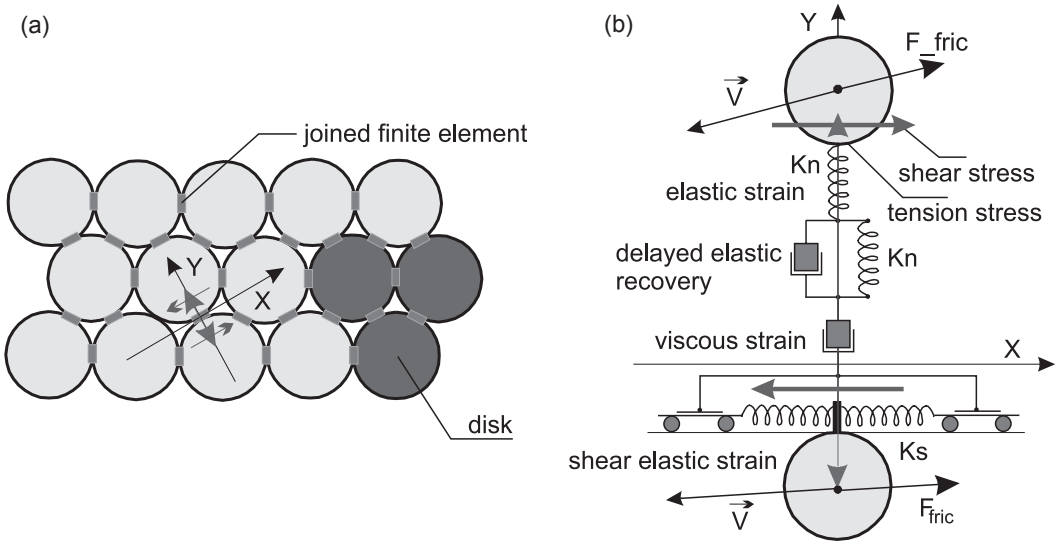

Fig. 3. (a) Package of the disk-shaped pieces. Every two coupled particles are bonded to each other by a finite element represented with a small solid rectangular. (b) Their spring analogy: a chart of background nonlinearity caused by delayed elastic recovery. Kn and Ks denote the disk instantaneous normal and shear stiffnesses, respectively, F_{fric} denotes the force of non-viscous friction.

based on viscous–plastic rheology where stress is linearly proportional to the strain for very slow strain rates.

In our study we assume that all disks in the system are regular, identical in size and with a unit thickness. The disks are glued together and uniformly fill out the Storfjorden area. Figure 3a shows the package of the disks covering Storfjorden and joined finite elements between them. In the quasi-static approach the length of every bond finite element is equal to 0.2 R, where R is the disk radius. The dynamic approach is based on a nonlinear strain–stress relationship applied in normal tension only. To achieve the compact package of the disks we applied a cellular construction algorithm of a uniform "honeycomb" grid when the density coefficient is equal to the ratio of the area occupied by disk-shaped rubbles to the total area:

$$d = 1 - \frac{2\sqrt{3} - \pi}{2\sqrt{3} + \pi} \approx 0.95 \qquad (1)$$

Every internal disk has six neighbours located in the vertexes of a regular hexagon. In fact, the shown density coefficient gives a theoretical estimation, which can never be achieved in mesoscale models, and approximately 5-6% of the investigated area remains disk-free. Bonds can transmit normal/shear stress, as well as the rotational moment preventing their relative sliding. Figure 3b illustrates the spring analogy of the system where the disk's normal and shear stiffnesses are denoted as k_n and k_s respectively. We neglected viscous interaction between the disks in the quasi-static approach.

In the dynamic approach discussed below there is a damping force calculated by the formula:

$$F_{fric,i} = -\mu \left| \vec{F}_{\Sigma,i} \right| \vec{V}_i \Big/ \left| \vec{V}_i \right|, \qquad (2)$$

where μ denotes the dimensionless damping coefficient, F_Σ is a total force acting on element i and $\vec{V}_i$ is the *i*-disk velocity. The damping coefficient can, for example, simulate a possible influence of a shallow sea floor when acting as an anchor for the ice cover. When the stress exceeds the normal/shear strength, the bond breaks. It leads to ice sheet destruction and causes ice drift. The linear strain–stress relationship is acceptable in the cases of slow strain rates and works well in the quasi-static approach but may become inapplicable in dynamic simulations. Laboratory experiments with columnar grained S2 ice samples distinctly indicate the nonlinear stress–strain relationship caused by the ice delayed-elastic strain and viscosity. The axial strain can be superimposed into three terms in accordance

with Sinha (1988) as follows:

$$e = e_e + e_d + e_v \,, \tag{3}$$

where e_e (23 %) is an instantaneous elastic strain, e_d (28 %) is a delayed elastic recovery and e_v (49 %) is a permanent or viscous strain. Sinha has proposed a strain–stress relationship for the columnar-grained S2 ice in the form:

$$e_e=\frac{\sigma}{E}\,,\ e_d=c\left(\frac{d_0}{d}\right)\left(\frac{\sigma}{E}\right)^s\cdot\left[1-e^{-(\alpha_T\cdot t)^b}\right],\ e_v=\dot{e}_{v0}\cdot t\cdot\left(\frac{\sigma}{\sigma_0}\right)^n \tag{4}$$

The physical parameters used are given in Table 1. Sinha's proposed nonlinear sea ice rheology was applied to a series of simulations (Zyryanov & Korsnes 2002) and calibrated to fit well the lab experiments.

The initial model configuration is shown in Fig. 4a. Wind stress is assumed to be the external drag force acting on the modelled ice sheet. In the beginning of the simulation there is no drag force and the system is in a static equilibrium.

Running the DEM sea ice destruction model

The quasi-static approach

Wind stress starts to increase slowly and uniformly in the selected direction. At every load-increasing step an equilibrium state is achieved characterized by the absence of all resultant forces acting on every disk in the system. In the code, the equilibrium is reached when the average ratio of all unbalanced forces to their maximum is less than $e=1\times10^{-3}$. Thus, there is no explicit time dependence and the simulation can be treated as a *quasi-static* process. Single disks or plates consisting of single disks can be separated from the main ice sheet by wind stress (i.e. destruction occurred) and drift away. In this case, the disks are simply deleted. Since this approach describes a time-independent process we allow the ice floes to stick together again, when two or more pieces touch in the process of simulation. From a physical point of view, such behaviour can be treated as the freezing together of isolated ice floes. A series of numerical experiments were performed with disk-shaped ice floes. The initial parameters and their values are shown in Table 2.

The dynamic approach with damping of disks movement in shallow areas based on nonlinear sea ice rheology

Grounded ice ridges on shallow shelves can influence the ice cover development process (Marchenko 2001). To reveal possible anchoring of the ice sheet to the sea floor we used in the dynamic model run a damping force based on the bathymetry data in Storfjorden. In shallow areas where the sea depth is less then 20 m mobile disks were assigned a damping coefficient ($\mu=0.8$) four times higher than in other areas of Storfjorden ($\mu=0.2$). The interaction between the ice floes is described by a nonlinear rheology approach investigated with laboratory ice specimens by Sinha (1988). It includes delayed elastic and viscous components of the total strain of the bond in tension (Fig. 3). The higher the strain rate, the more pronounced nonlinearity in the stress–strain relationship was observed (Cole et al. 1998). The idea behind the dynamic application of DEM based on the real sea ice rheology is to determine the role of nonlinearity in geoscale simulations of sea ice destruction. However, for

Table 1. The parameter values used in the nonlinear strain–stress dynamic simulation.

Parameter	Description	Value
k_n	bond stiffness	5×10^9 Nm^{-2}
C	material constant	9×10^{-3}
B	time exp. for delayed elastic strain	0.34
a_T	material constant	2.5×10^{-4} s^{-1}
D	an average grain diameter	1 mm
D_0	grain diameter unit	1 mm
S	stress exp. for grain-bound sliding	1
N	degree of viscosity power law	3
e_{v0}	viscous strain rate	1.76×10^{-7} s^{-1}
normal/shear strength	constant strength	$1\text{-}5\times10^8$ Pa

an ice cover failure, it is important to know the ice strength as well. Experiments with ice under tension indicate that the ice strength is particularly highly sensitive to the strain rate. An empirical power ratio is proposed that relates the maximum stress of the ice specimen in tension (e.g. ice strength) to its strain rate.

Simulation results compared with ERS-2 SAR images

Figure 4b-c show the modelled polynya outlines where the wind direction changes discretely with a step of 11.25° in the sector from 0° N to 45° N. Figure 4b represents the equilibrium stages when the remaining ice sheet is equal to about 85% of the original, whereas Fig. 4c corresponds to 50% of ice sheet destruction. A fixed area of the remained ice sheet is achieved with different wind drag force magnitudes and is dependent upon the wind azimuth. Figure 5 indicates the development of the polynya versus the wind stress magnitude for different wind directions. The bigger the ice-free area, the more pronounced difference in applied stress for two extreme wind azimuths, 0° N and 45° NE, is observed. Northerly winds open a polynya area about 30% larger than north-easterly winds with the same drag force magnitude.

Figure 6a shows a typical ERS-2 SAR view of the Storfjorden ice condition during the winter 1997/98. The two original SAR scenes of 100×200 km^2 are low resolution images (LRI). The LRI format is provided by the Tromsø Satellite Station and has a pixel resolution of 100 m. The presented scenes are dated 12 April 1998, when a large polynya occurred over the centre of the fjord. Fast ice was present over the whole shallow northern part of Storfjorden and along the Spitsbergen coast. A manual segmentation of the ERS-2 SAR image into fast ice, pack ice and polynya was performed for Fig. 6b with the help of sequential images to detect temporal changes (Haarpaintner et al. 2001). The modelled boundaries of 50% ice sheet break-up (Fig. 4c) agree strongly with the observed boundaries of the polynya during winter 1997/98. The first step of each model run has been initialized with the standard parameters (Table 1) and an average wind speed of 6 m/s. The ice cover fluctuations shown in Figs 4b-c correspond to wind speed variations of 5.72-6.4 m/s and 6.7-10.8 m/s, respectively, whereas daily averaged meteoro-

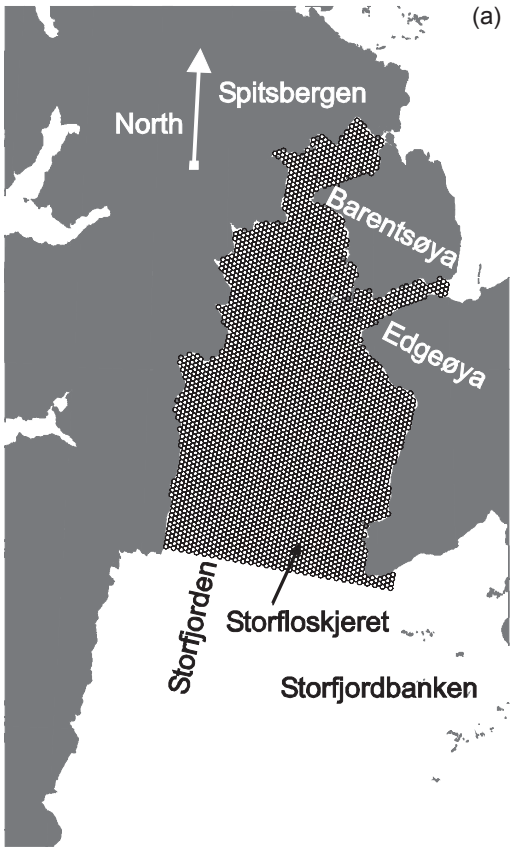

Fig. 4. (a) The initial model configuration. Coupled disks uniformly fill out the Storfjorden area. (b, c, opposite page): The statistical variations of the polynya outlines due to the wind direction variations from 0° N to 45° NE (number of simulation series N = 5). The colour bars show the observed simulations variability: 0 indicates the absence of ice floes, whereas 1 corresponds to their presence in all simulation series. In (b) approximately 85% of the original number of ice floes remains. In (c) approximately 50% of the original number of ice floes remains.

Table 2. The parameter values used in the quasi-static model run.

Parameter	Value
Number of disk-shaped particles in the system	3871
Disk radius	0.7 km
Disk normal stiffness, k_n	$1\text{-}5 \times 10^9$ Nm^{-1}
Disk shear stiffness, k_s	$1\text{-}5 \times 10^9$ Nm^{-1}
Normal/shear strength	$1\text{-}5 \times 10^8$ Pa
Wind azimuth, degrees (sector from N to NE)	0 N, 11.25 NNE, 22.5 NNE, 33.75 NE, 45 NE

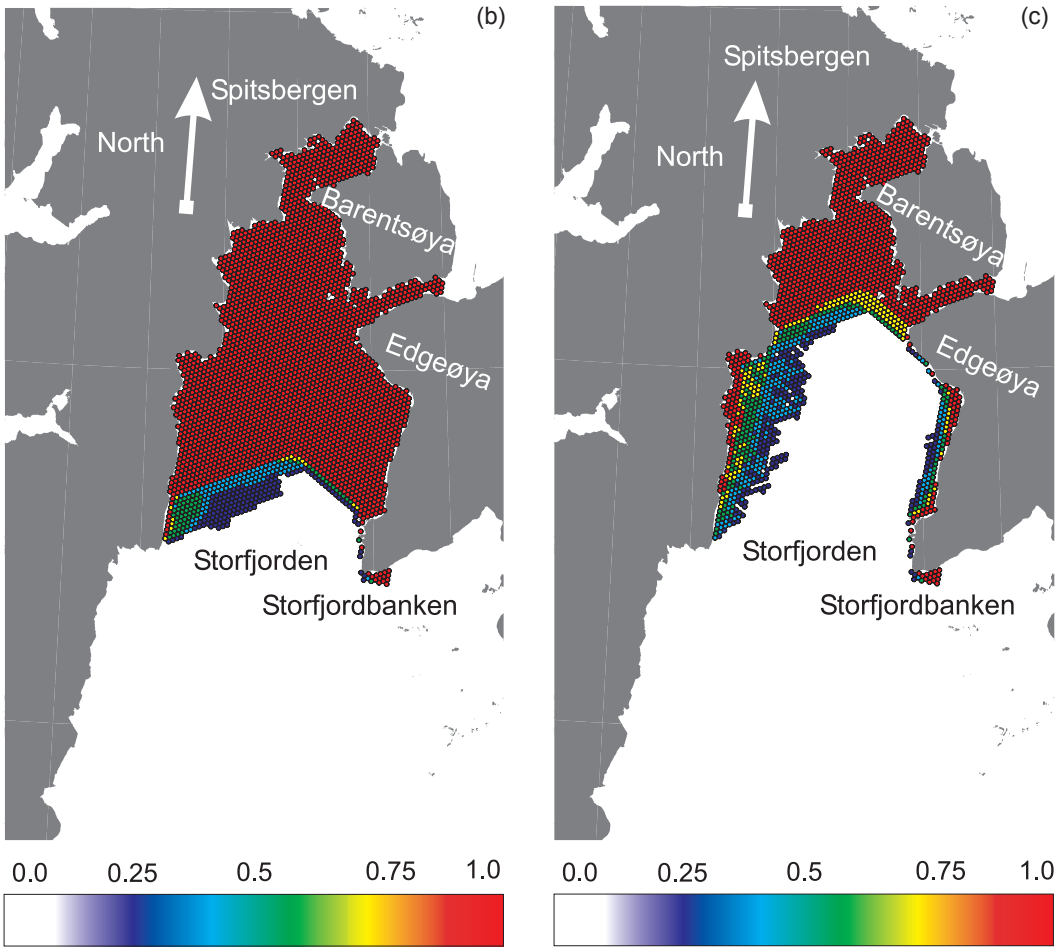

logical data from the Hopen meteorological station (Fig. 2a) indicate wind gusts of ca. 10 m/s at the end of January 1998. As evident in Fig. 4c, the northern modelled boundary between Agardhbulkta and Freemansundet fits the observations perfectly. The simulation results also show that small reefs (e.g. Storfloskjeret, located at the mouth of the fjord; Fig. 4a) do not appear to strongly influence the polynya development. At least in a series of numerical experiments with truly mechanical features of real sea ice we noted that separate barriers, anchoring the ice sheet, do not essentially prevent the ice cover from destruction. This could indicate that the fjord geometry combined with the northerly wind stress are dominant parameters in the break-up process of the polynya compared to the hypothetical influence of the tidal currents through Freemandsundet.

Role of the damping of ice floes and sea ice rheology

Applying a non-uniform damping force of moving particles in shallow areas and a nonlinear ice rheology may lead to qualitatively different simulation results. Figure 7a indicates the dynamic simulation result when the damping coefficient is non-uniform with a ratio of 0.2/0.8 in deep/shallow areas, whereas Fig. 7b represents a uniform of 0.2 damping throughout the modelled ice cover in the quasi-static approach. We considered a rapid ice cover destruction process in dynamics, when the sum of the delayed elastic and viscous components dominate the total ice strain by more than 60 %. Their influence is revealed in smoother free boundaries of the ice sheet. The role of

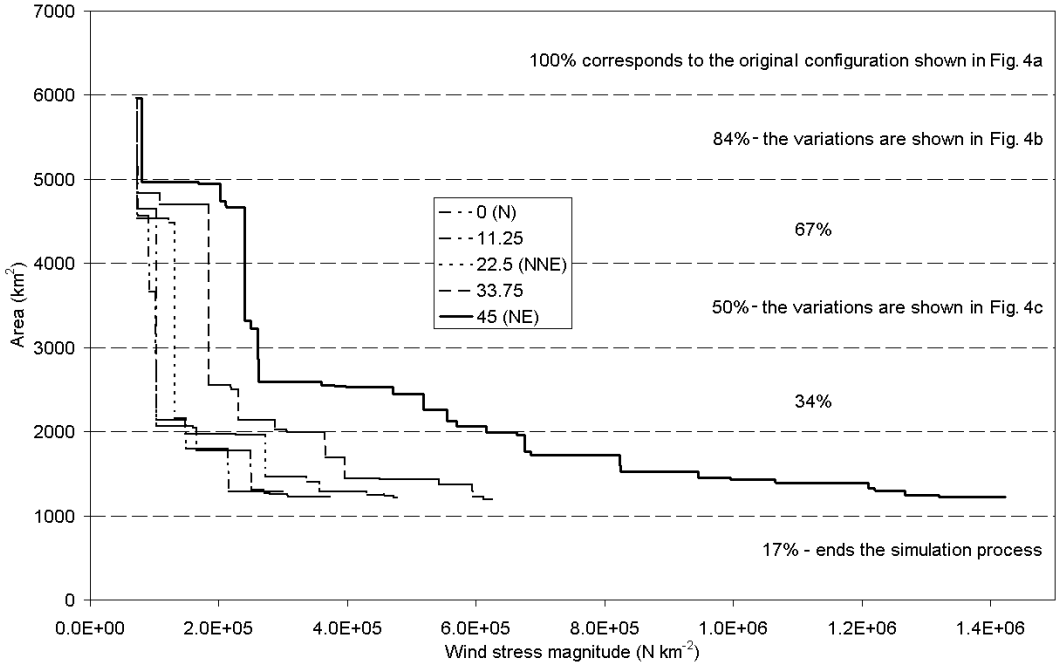

Fig. 5. Graph of area occupied by ice floes (km^2) versus wind stress magnitude for different wind directions. The wind direction varies from 0° N to 45° NE.

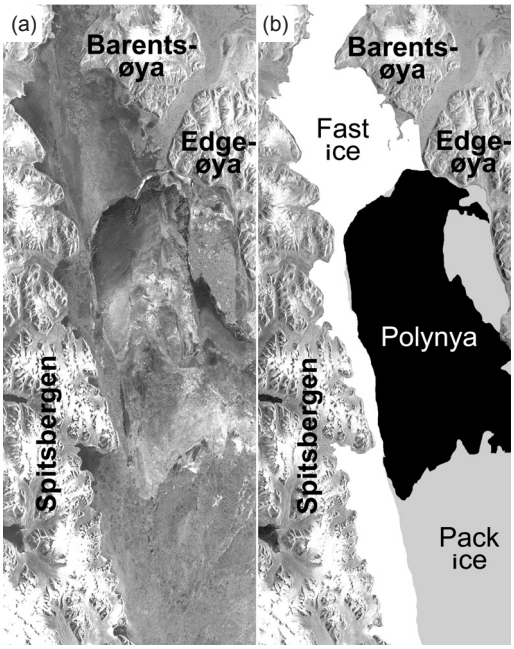

Fig. 6. (a) The Storfjorden ice conditions on 12 April 1998 observed by ERS-2 SAR (original data © ESA [1998], distributed by Eurimage [TSS]). (b) A manual segmentation of the ERS-2 SAR image into fast ice (white), pack ice (gray) and polynya (black) that includes open water and thin ice.

damping is best revealed near the western coast of Edgeøya. It corresponds to the area of pack ice in Fig. 6b, where the SAR-2 image is manually segmented into fast ice, pack ice and ice-free areas.

Conclusions

The aim of this work was to consider some possible scenarios of polynya formation due to the wind drag force in Storfjorden, Svalbard, and an overall validation of the DEMs for this region. We focused on the phenomenon of a latent heat polynya that opened mechanically under wind stress. In this paper, quasi-static and dynamic disk-shaped simulations were used to model the polynya opening and development. The simulation of an ice-free area development began with a uniform cover consisting of disk-shaped particles coupled together. A homogeneous (fixed direction) and uniformly increased external drag force was applied to the system of bonded ice floes. The ice cover started to break up and ice-free zones appeared.

A series of numerical experiments were performed to establish the dependence of the size of the ice-free area on the wind stress. These exper-

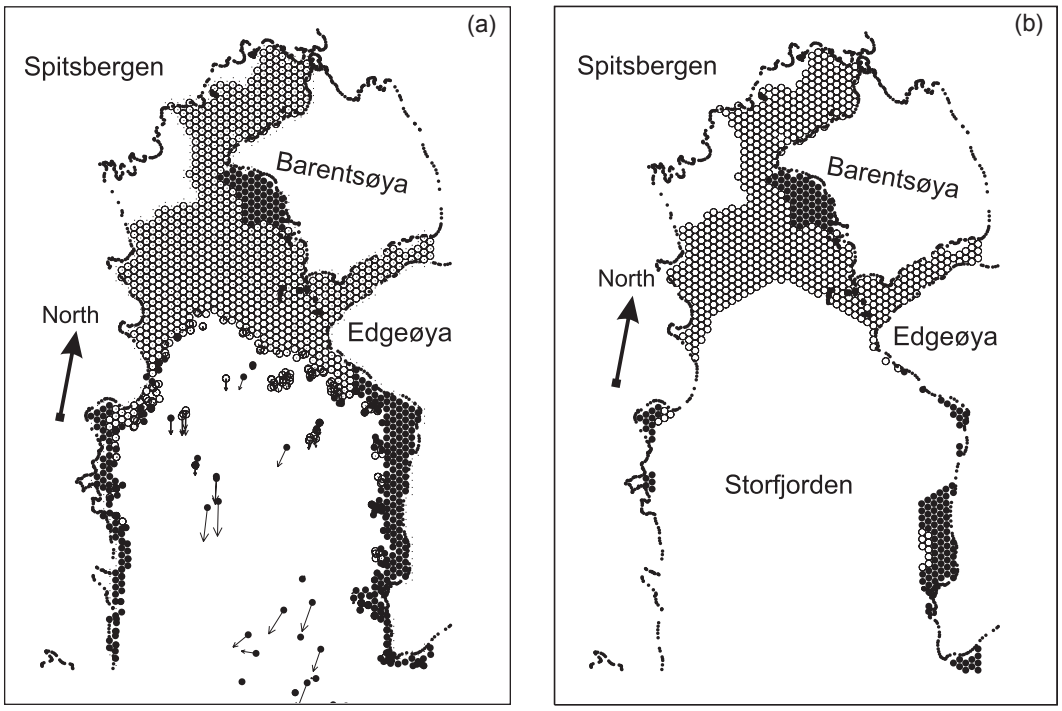

Fig. 7. (a) The simulation results of the dynamic run of the model with heterogeneous damping coefficients based on a nonlinear stress–strain relationship and a constant ice strength. In shallow areas (depth less then 20 m—black zones in the illustration) the damping coefficient is equal to 0.8; for the rest of Storfjorden the damping coefficient is equal to 0.2. The wind stress is constant of 6.4 m/s directed from the north. The simulation time is equal to 18.3 s. (b) The simulation results of quasi-static run of the model with homogeneous damping coefficients based on linear theory and a constant ice strength: the damping coefficient is equal to 0.2 throughout the modelled ice sheet. The wind stress is constant of 6.4 m/s directed from the north.

iments show that for the larger ice-free areas in Storfjorden (>40%) the wind stress magnitude, which leads to such configurations, nonlinearly increases with the increase of the wind stress azimuth (see Fig. 5).

Finally, we compared visually the simulation results with the satellite observation of the Storfjorden polynya opening on 12 April 1998 derived by ERS-2 SAR. The comparison shows that the geometry of Storfjorden as well as its shallow areas generally play a significant role in the geometry of the polynya boundaries. This approach could potentially be applied to estimations of the size of ice-free areas in Storfjorden and the polynya outline based on the meteorological data in subsequent years. However, more remote sensing observations are necessary for a reliable model validation during different meteorological conditions.

Acknowledgements.—The work upon which this paper is based was carried out while all three authors were at the Norwegian Polar Institute (NPI). The work has been funded by grant no. 128087/730 from the Research Council of Norway, under contract with the NPI. We wish to express our gratitude to Alexey Marchenko for his important comments and directions and to our colleague Harvey Goodwin (NPI) for technical assistance in preparing this manuscript. We thank two anonymous reviewers for constructive suggestions improving the manuscript.

References

Banke, E. G. & Smith, S. D. 1973: Wind stress on Arctic sea ice. *J. Geophys. Res. 78(33)*, 7871–7883.

Cole, D. M., Johnson, R. A. & Durell, G. D. 1998: Cyclic loading and creep response of aligned first-year sea ice. *J. Geophys. Res. 103(C10),* 21 751–21 758.

Haarpaintner, J. 1999: The Storfjorden polynya: ERS-2 SAR observations and overview. *Polar Res. 18*, 175–182.

Haarpaintner, J., Gascard, J. C. & Haugan, P. M. 2001: Ice production and brine formation in Storfjorden, Svalbard. *J. Geophys. Res. 106(C7)*, 14 001–14 013.

Hansen, E. & Løset, S. 1999a: Modelling floating units

moored in broken ice: model description. *Cold Reg. Sci. Technol. 29*, 97–106.
Hansen, E. & Løset, S. 1999b: Modelling floating units moored in broken ice: comparing simulations with ice tank tests. *Cold Reg. Sci. Technol. 29*, 107–119.
Hopkins, M. A. 1993: A mesoscale simulations of the Arctic ice pack. In J. P. Dempsey et al. (eds.): *Ice mechanics 1993. ASME AMD 163*. Pp. 85–96. New York: Americal Society of Mechanical Engineers.
Hopkins, M. A. 1996: On the mesoscale interaction of lead ice and floes. *J. Geophys. Res. 101(C8)*, 18 315–18 326.
Hopkins, M. A. & Hibler, W. D. 1991: Numerical simulations of a convergent system of ice floes. *Ann. Glaciol. 15*, 26–30.
Hopkins, M. A., Hibler, W. D. III & Flato, G. M. 1991: On the numerical simulation of the sea ice ridging process. *J. Geophys. Res. 96(C3)*, 4809–4820.
Løset, S. 1994: Discrete element modelling of a broken ice field. Part I: model development. *Cold Reg. Sci. Technol. 22*, 339–347.
Marchenko, A. 2001: Model for the formation of hummocks in a drifting ice cover. *J. Phys.-Uspekhi 44*, 315–320.
Midttun, L. 1985: Formation of dense bottom water in the Barents Sea. *Deep-Sea Res. 32*, 1233–1241.
Omstedt, A., Nyberg, L. & Lepparanta, M. 1996: On the ice-ocean response to wind forcing. *Dyn. Meteorol. Oceanogr. 48*, 593–606.
Overland, J. E. 1985: Atmospheric boundary layer structure and drag coefficient over sea ice. *J. Geophys. Res. 90(C5)*, 9029–9049.
Overland, J. E. 1994: Geostrophic drag coefficients for the central Arctic derived from Soviet drifting station data. *Tellus 46a*, 75–85.
Pease, C. H. 1987: The size of wind-driven coastal polynyas. *J. Geophys. Res. 92(C7)*, 7049–7059.
Quadfasel, D., Rudels, B. & Kurz, K. 1988: Outflow of dense water from Svalbard Fjord into the Fram Strait. *Deep-Sea Res. 35(7)*, 1143–1150.
Savage, S. B. 1992: *Marginal ice zone dynamics modelled by computer simulations involving floe collision. Technical Report. Ottawa:* Institute of Mechanical Engineering. National Research Council.
Sayed, M., Venkata, R. N. & Savage, S. B. 1995: Yield conditions of an assembly of discrete ice floes. In: *Proceedings of the Fifth International Offshore and Polar Engineering Conference (ISOPE 95). Vol. 2.* Pp. 330–335. The Hague: International Society of Offshore and Polar Engineers.
Sinha, N. K. 1988: Crack-enhanced creep in polycrystalline material: strain-rate sensitive strength and deformation of ice. *J. Mater. Sci. 23*, 4415–4428.
Smith, S. D., Muench, R. D. & Pease, C. N. 1990: Polynyas and leads: an overview of physical process and environment. *J. Geophys. Res. 95(C6)*, 9461–9479.
Willmot, A. J., Maqueda, M. A. & Darby, M. S. 1997: Model for the influence of wind and oceanic currents on the size of a steady-state latent heat coastal polynya. *J. Phys. Oceanogr. 27*, 2256–2275.
Zyryanov, D. & Korsnes, R. 2002: A numerical model for simulation of sea ice destruction due to external stress in geoscale areas. In H. Konietzky (ed.): *Presentations from the conference. The 1st International PFC Symposium, Gelsenkirchen, Germay, 2002. Numerical Modeling in Micromechanics via Particle Methods.* CD-ROM. Minneapolis: Itasca Consulting Group, Inc.

Appendix 1

The physics of the problem are represented using several parameters to which the solution may be sensitive. Therefore, the sensitivity analysis should be performed to eliminate possible instabilities in the model behaviour. These variations can be caused by: (1) computational abnormalities closely related to the calculation algorithm, in most cases treated as errors; (2) objective motives, e.g. sensitivity to the wind direction and/or simulation parameter variations, such as yield factors etc. One should note that the splitting of the model parameters into these two groups is a complicated problem and requires in situ data processing during lenghty time periods. The phenomenon of the Storfjorden polynya became the centre of attention relatively recently (Midttun 1985; Quadfasel et al. 1988). A lack of field data, especially satellite observations showing the opening of the polynya, is a significant barrier for further model development and verification.

To reveal the sensitivity of the system to the parameter variations, we changed the elastic properties of the ice floes as well as the normal/shear strength values (Table 3) in a wide range. Variations of ice floe stiffness (k_{ns}) from 1.0 to 5.0×10^9 Nm^{-1} produced no significant changes in the results, indicating only a slight decrease of the wind stress needed for the polynya to exist for lower values of k_{ns}.

The disk stiffnesses variations as well as the different model normal/shear strengths are shown in Table 3. The results of the simulation show that variations of ice floe stiffness have no significant effect on the ice-free area other than a small diminution of this area for the lower values. When the normal/shear strength increases, wind drag force leading to the ice sheet destruction increases as well.

Table 3. Sensitivity of the model to the wind direction and parameter variations.

Wind stress magnitude (Nkm^{-2})	Wind direction (azimuth degrees)	K_n (Nm^{-1})	K_s (Nm^{-1})	Normal/shear strength (Pa)	Area occupied by ice floes (km^2) $S = <\#\ of\ disks> (\sqrt{3} + \pi/2) r^2$
1.0×10^5	0° N	5×10^9	5×10^9	1×10^8	$2.2x \times 0^3$ (36 %)
1.0×10^5	11.25° N	5×10^9	5×10^9	1×10^8	4.84×10^3
1.0×10^5	22.5° N - NE	5×10^9	5×10^9	1×10^8	4.76×10^3
1.0×10^5	33.75° N - NE	5×10^9	5×10^9	1×10^8	5.05×10^3
1.0×10^5	*45° N - NE*	*5×10^9*	*5×10^9*	*1×10^8*	*5.23×10^3*
0.8×10^5	0° N	1×10^9	1×10^9	1×10^8	2.38×10^3 (38 %)
0.8×10^5	11.25° N	1×10^9	1×10^9	1×10^8	4.76×10^3
0.8×10^5	22.5° N - NE	1×10^9	1×10^9	1×10^8	4.87×10^3
0.8×10^5	33.75° N - NE	1×10^9	1×10^9	1×10^8	5.13×10^3
0.8×10^5	45° N - NE	1×10^9	1×10^9	1×10^8	5.06×10^3
1.03×10^5	0° N	5×10^9	5×10^9	5×10^8	2.43×10^3 (39 %)
1.03×10^5	11.25° N	5×10^9	5×10^9	5×10^8	4.71×10^3
1.03×10^5	22.5° N - NE	5×10^9	5×10^9	5×10^8	4.76×10^3
1.03×10^5	33.75° N - NE	5×10^9	5×10^9	5×10^8	5.05×10^3
1.03×10^5	45° N - NE	5×10^9	5×10^9	5×10^8	5.18×10^3